Renewable Energy 145 (2020) 2694–2706

Contents lists available at ScienceDirect

Renewable Energy

journal homepage: www.elsevier.com/locate/renene

Alternative operational strategies for wind turbines in cold climates

D.B. Stoyanov, J.D. Nixon*

Faculty of Engineering, Environment and Computing, Coventry University, 1 Gulson Road, Coventry, CV1 2JH, UK

ARTICLE INFO

Article history:
Received 10 April 2019
Received in revised form
1 August 2019
Accepted 5 August 2019
Available online 6 August 2019

Keywords:
Ice accretion
Wind power
Wind energy
Tip-speed ratio (TSR)
Aerodynamics
Icing events

ABSTRACT

Around a quarter of the global wind energy capacity is operating in cold climates, where ice accretion can damage wind turbines, cause safety concerns and reduce power output. In this paper, alternative operational strategies to reduce ice build-up and increase power output are studied. The alternative strategies are achieved by making tip-speed ratio (TSR) modifications both during and after an icing event. To compare different TSR strategies, the concept of an energy payback time is outlined, which is used to determine when an alternative strategy outperforms a turbine's normal design strategy. The method is demonstrated using the NREL 5 MW reference wind turbine for twelve different icing conditions, encompassing different temperatures, wind speeds, droplet diameters and liquid water contents. The results indicate that for short and severe icing events, an alternative TSR strategy will start producing more energy than a conventional design strategy within 0.5–2.5 h after icing and decrease ice accumulation by approximately 25–30% per blade. The method presented in this study will enable more effective operational control strategies to be deployed for minimising ice-induced power losses and ice accretion at wind farms located in cold climates.

1. Introduction

By the end of 2017, the global wind energy capacity was approximately 540 GW [1]. Nearly a quarter of the installed capacity is expected to be at risk of icing due to cold climate (CC) conditions [2]. Locations classified as CCs are typically characterised by a high wind resource availability [3]. However, in such conditions, the efficiency of wind turbines can be severely compromised by the prevalence of icing, reducing power output [4–7], causing structural damage and decreasing wind turbines' life span [7,8]. Ice induced power losses can be extremely variable depending on location, wind turbine scale and weather conditions [7,9]. This can make it difficult deciding where to locate a wind turbine and how to operate it in CCs. As a result, annual losses reported for wind turbines in CCs can often reach 20% [6].

Most commercial wind turbine blades are designed as lift generating devices and ice build-up on the aerofoils typically decreases lift and increases drag. This reduction in aerodynamic efficiency is generally well known from previous research on aircraft icing [10–13], and many studies are now focusing on the implications for the wind energy industry.

A significant amount of research has been carried out on how ice forms on wind turbines [11,14], impacts power output [6,13,15] and affects structural robustness [14,16]. Thus, it has been established how much more severe icing is for longer icing events, larger water droplet sizes and liquid water contents, smaller chord lengths and higher wind speeds. In addition, it is known that ice thickness increases approximately linearly from the root to the tip of the blade when considering a 2D analysis and not accounting for ice shedding [16]. Although more research is needed to substantiate these results and classify them in a useful database, there is a particular need to utilise these findings and search for more efficient approaches to operate wind turbines in icing conditions [17]. An efficient wind turbine operational strategy can minimise annual power losses, prevent structural damage and reduce wind turbine downtime. However, there are only a limited number of studies that have looked at improving wind turbines operational efficiency in icing conditions by applying different tip-speed ratio (TSR) strategies.

Homola et al. [18] and Zanon et al. [19] investigated the operation of the National Renewable Energy Laboratory (NREL) 5 MW reference wind turbine in icing conditions. Both studies analysed the performance of the wind turbine considering the torque-speed curve and the torque-speed controller. Homola et al. [18] simulated the iced performance of the wind turbine after a one-hour long icing event, operating the wind turbine either by adapting the

* Corresponding author.
E-mail address: jonathan.nixon@coventry.ac.uk (J.D. Nixon).

https://doi.org/10.1016/j.renene.2019.08.023
0960-1481/

Nomenclature

Variables

a	Axial induction factor (−)
a′	Tangential induction factor (−)
c	Aerofoil chord length (m)
Cp	Power coefficient (−)
E	Energy (MWh)
LWC	Liquid water content (kg.m^{-3})
M	Mass (kg)
MVD	Median volume diameter (m)
P_W	Wind power (W)
r	Blade radius (m)
T	Temperature (°C)
t	Time (h)
TSR	Tip-speed ratio (−)
V	Wind speed (m.s^{-1})

Greek

ρ	Air density (kg.m^{-3})
ω	Rotor Rotational Speed (rad.s^{-1})

Subscripts

AI	After icing
DI	During icing
EPB	Energy payback
M	Modified operational strategy
R	Reference operational strategy
rel	Relative to the blade

Acronyms

AoA	Angle of attack
BEMT	Blade element momentum theory
CC	Cold climate
NREL	National Renewable Energy Laboratory

torque-speed controller to the iced-torques-speed curve or by modifying the controller to maintain the TSR at its design value. When examining the wind turbine power curve for the iced blade and bypassing the controller, a 10% higher achievable power output for velocities between 7 and 13 m s^{-1} was reported, while slightly higher power losses were seen for wind speeds of 3 and 6 m s^{-1}. As the study focused on a single icing condition, the authors highlighted the need for further analysis of more severe icing cases. Zanon et al. [19] analysed the wind turbine's performance during an active icing period and showed the influence of three different TSR operational strategies on the ice-induced power losses. The study showed how the ice-induced losses can be mitigated by reducing the TSR during an icing event. However, a reduction in the ice-induced power losses, does not necessarily mean that overall energy generation would be increased.

By reducing the TSR during an icing event to minimise ice build-up, the reference TSR could be restored once an icing event ends to improve performance [20]. However, the reference TSR may no longer be the best post-icing event operational strategy due to ice remaining on the blades and changes in aerodynamic behaviour. To determine if gains in energy generation can actually be achieved, a turbine's performance needs to be analysed throughout and immediately after an icing event. This approach could also be used to implement an operational strategy to both reduce ice build-up during an event and maximise post-icing event power output. Moreover, a method for comparing and evaluating different TSR operational strategies is needed and the performance analysis needs to be applied for a wide range of different icing conditions.

This study aims to establish a method for evaluating different operational strategies based on tip-speed ratio modifications made both during and after an icing event. This is achieved by introducing the concept of an energy payback time, which is based on the time taken for an alternative TSR strategy to start producing more energy than the reference operational regime after the end of an icing event. By considering a wide range of different icing events, wind speeds and ambient temperatures, the study sets out to determine when an alternative operational strategy should be used to reduce ice build-up during an icing event and increase energy yield once an event ends.

Section 2 specifies the methods used to carry out the study including definition of the icing model, iced blade aerodynamic performance, icing events considered and energy payback parameter based on ice accretion and modified power coefficients. The results and suggestions for further work are discussed in Section 3, and the paper's conclusions are provided in Section 4.

2. Method

In this study, three typical icing events are considered to evaluate a number of different operational strategies based on varying tip-speed ratios. Furthermore, each event is tested for three different wind speeds (5, 7 and 10 m s^{-1}) and two ambient temperatures (−5 and −10 °C). To simulate ice formation during these events, LewINT® ice accretion software is used as it is the most widely established tool for generating 2D ice shapes on aerofoils and it has been validated extensively for aircraft icing [21,22]. LewINT® is based on source and dipole singularities superposition panel method to obtain flow velocities, which are used to calculate droplet trajectories, aerofoil surface water fluxes and energy balance for the ice shape calculations. Qblade is utilised for the power performance analysis [23]; it incorporates Blade Element Momentum Theory (BEMT) for power analysis and XFoil [24] for the aerodynamic analysis, which utilises vortex and source singularities panel method together with integral boundary layer method. Both methods have been widely used and allow for relatively low computationally intensive simulations to be carried out. The wind turbine chosen for the study is the NREL 5 MW reference wind turbine [25], as it is commonly used in the literature for this type of study.

2.1. Ice accretion modelling

To reduce the number of required simulations, four sections of the wind turbine blade are modelled to determine the ice accumulation along its length during the icing events. Fig. 1 shows the sections, which are considered between the half-span and the full span of the blade: sections A, B, C and D. The distances from the blades centre of rotation are as follows: l_1 is 0.52r, l_2 is 0.65r, l_3 is 0.80r and l_4 is 0.94r with *r* being the local blade radius. The hub radius, L_H, and blade length, L_B, are 1.5 m and 61.5 m, respectively. The aerofoils corresponding to the chosen blade sections are DU 91W225 for Section A, DU 93W21LM for Section B and NACA 64618 for sections C and D. As minimal icing occurs on the inner-blade sections, they have not been considered during the ice accretion simulations [19].

The ice formation analysis has been conducted using the 2D

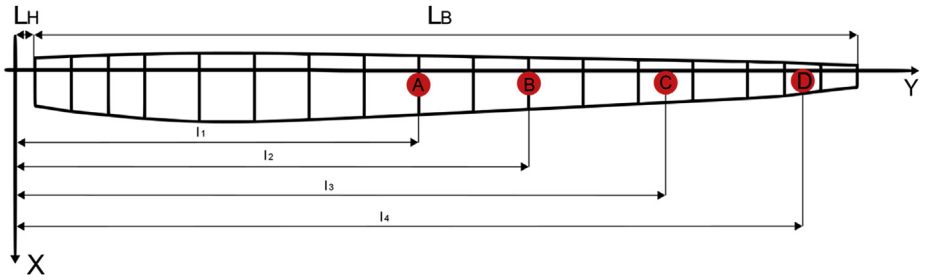

Fig. 1. Discretised NREL 5 MW blade and the selected 2D sections for ice accretion analysis.

aerofoil sections at each of the four discretised locations. Symmetrical ice deposition across the turbine's three blades is assumed with uniform ice geometry for each iced section. The relative speed to the blade sections is calculated using classic BEMT theory, Eq. (1), where V_{rel} is the relative speed to the blade, V is the wind speed, ω is the rotational speed of the rotor, r is the local blade section radius, and a and a' are the axial and tangential induction factors, respectively. The ice mass is estimated by using the predefined ice density of 917 kg m^{-3} in lewINT [21].

$$V_{rel} = \sqrt{(V\,(1-a))^2 + (\omega r(1+a'))^2} \tag{1}$$

Using low computationally intensive tools allows for the simulation of a variety of icing events in a relatively short time. However, this does reduce the accuracy of the aerodynamic analyses. XFoil is a two-dimensional tool, which incorporates the integral boundary layer equations in the viscous boundary layer and potential flow equations in the outer inviscid region; the two regions are coupled using viscous-inviscid interaction scheme. Due to the use of XFoil and 2D analysis, increased uncertainty is expected for cases where separated flow occurs, e.g. for high angles of attack (AoA) or highly irregular ice shapes.

2.1.1. Icing events definition

To study wind turbine performance during different in-cloud icing events, encompassing rime, mixed and glaze icing conditions, a number of icing events are defined based on published experimental [26] and field data [27,28]. The different ice modelling parameters that need to be considered include liquid water content (LWC), median volume diameter (MVD) and icing event duration (t_{Event}). Each parameter can vary widely for different locations and especially for different orographic features. In-cloud icing conditions are mostly pronounced in hilly and mountainous terrains, where wind turbine blades can reach the low-level cloud base (300–1200m) during winter months [28]. A typical MVD for in-cloud icing is 20×10^{-6} m [26], but it can range from $10–35 \times 10^{-6}$ m [28]. The LWC is normally 3×10^{-4} kg m^{-3} [26], and ranges from $0.4–3.5 \times 10^{-4}$ kg m^{-3} [28,29]. Ice events tend to be shorter for larger liquid water contents and size droplets [29,30] and typical durations range from 20 min to 48 h, while in some cases up to several weeks [29].

During an icing event, wind speed (V) and ambient temperature (T) significantly influence the type of ice being accreted. Thus, three icing events (defining LWC, MVD and duration) are chosen along with different wind speeds and ambient temperatures that are most likely to occur. Table 1 shows icing event A (LWC of 5×10^{-4} kg m^{-3} and MVD of 25×10^{-6} m), B (LWC of 3×10^{-4} kg m^{-3} and MVD of 20×10^{-6} m) and C (LWC of 0.4×10^{-4} kg m^{-3} and MVD of 12x10^{-6} m), which are modelled at different temperatures (−5 °C and −10 °C) and wind speeds (5, 7 and 10 m s^{-1}) giving a total of 12 different icing cases. Event A represents the harshest conditions, which typically occur for a relatively short duration, and events B and C are mild and light conditions respectively.

2.2. Operational strategy

The control parameter used in this study is TSR and its setting during (TSR_{DI}) and after (TSR_{AI}) an icing event. The TSR changes can be implemented by either prescribing constant TSR during the event or by adapting the torque-speed controller to the iced torque-speed curve [19]. In this work, steady state simulation of the icing process and the aerodynamic effects is considered, similarly to previous research [16,18]. It is assumed that the TSR during icing will remain constant as the icing durations in the current study are short enough and the natural degradation of the TSR will be small [19]. The possible TSR values that can be set are chosen according to the rated (maximum) rotational speed (seldom synchronous and asynchronous generators are operated above their rated speed) and the minimum rotational speed, required for energy generation. Considering the NREL 5 MW generator [25] with a minimum RPM of 670 and maximum of 1173.7RPM, the possible TSR limits (TSR_{Min} and TSR_{Max}) for operation can be determined (see Fig. 2). The reference TSR design strategy is shown by TSR_R and Fig. 2b shows how the coefficient of power (Cp) varies at different TSR settings for a non-iced blade. During an icing event, it is assumed that the controller will allow intentional energy yield reduction by reducing the tip-speed ratio, thereby reducing ice accretion and enabling an improved Cp to be obtained once the event finishes [14].

2.3. Energy payback time

The energy payback time, t_{EPB}, defines how long it will take an alternative modified operational strategy (TSR_M) to start producing more power than the turbine's reference strategy (TSR_R). Fig. 3a depicts the reduction of the instantaneous power output during an icing event by operating with an alternative TSR_{DI}, and the potential for improving performance at the end of an icing event by increasing the TSR_{AI} due to less accreted ice and better power characteristics. To compare a modified and reference operational strategy, the cumulative energy harvested during and after an event needs to be determined (see Fig. 3b). The cumulative energy produced during icing, E_{DI}, is found from the available power in the wind, P_w, and the power coefficient, Cp, which varies throughout the duration of the icing event and depends on the chosen TSR (Eq. (3)). P_W is defined by the air density, ρ, wind speed, V, and wind turbine blade radius, r (Eq. (2)).

$$P_W = 0.5\rho V^3 \pi r^2 \tag{2}$$

$$E_{DI} = \int P_w Cp_{(TSR,t)}\,dt \tag{3}$$

Table 1
Definition of icing events A, B and C, at different wind speeds (V) and temperature (T).

Event, V, T	LWC (kg.m^{-3})	MVD (μm)	Duration, t_{Event} (s)	(V (m.s^{-1}))	T (°C)
A1010	5	25	1	10	−10
A105	5	25	1	10	−5
A710	5	25	1	7	−10
A75	5	25	1	7	−5
A510	5	25	1	5	−10
A55	5	25	1	5	−5
B1010	3	20	4	10	−10
B710	3	20	4	7	−10
B75	3	20	4	7	−5
B510	3	20	4	5	−10
C105	0.4	12	4	10	−5
C1010	0.4	12	4	10	−10

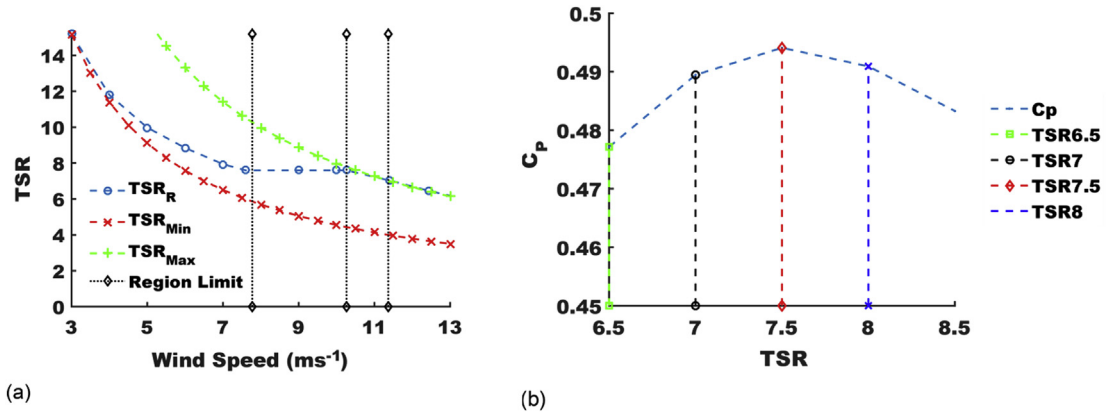

Fig. 2. a–b: NREL 5 MW reference wind turbine TSR operational limits defined by the limiting rotational speeds of the electrical generator (a) and how the power coefficient varies at different TSR (b).

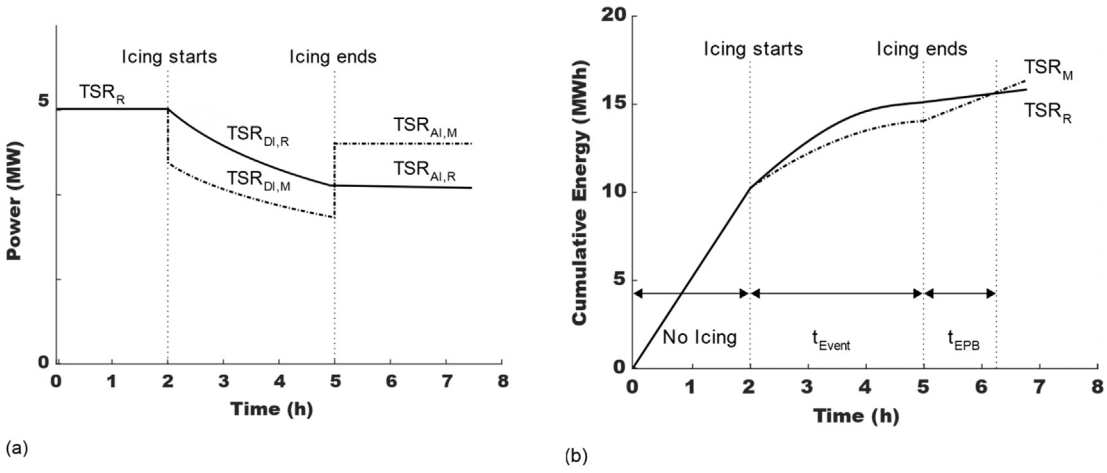

Fig. 3. a–b: Power output (a) and cumulative energy (b) during and after an icing event for a wind turbine operating with a reference (TSR_R) or modified (TSR_M) tip-speed ratio strategy.

The assumption is made that for a short period (<48 h) after the end of an icing event, no significant ice melting or shedding will occur. This assumption is based on the consideration of winter anticyclone weather conditions with low temperatures and wind speeds that could span up to a week or more after an in-cloud icing event [31]. The coefficient of power will remain constant, if the assumption is made that the iced blade geometry will not change significantly soon after the end of an icing event. Thus, the cumulative net energy output will be linear as *Cp* defines the rate of energy yield. The energy produced after an icing event by the reference ($E_{AI,R}$) and a modified ($E_{AR,M}$) operational strategies can be represented by equations Eq. (4) and Eq. (5), respectively. The rate of cumulative energy after the icing event is calculated in addition to the total energy produced during the icing event (E_{DI}); $E_{DI,R}$ and $E_{DI,M}$ are respectively the cumulative energy produced during the icing event for the reference and modified operational strategies.

The time taken for the modified strategy to payback the lost energy during icing is determined when $E_{AI,R}$ equals $E_{AI,M}$; making t_{EPB} the subject of the equation results in Eq. (6). When estimating t_{EPB}, it should be noted that the results are only an indication for the potential effectiveness of an alternative strategy and extremely large values would suggest that alternative solutions to the TSR strategy should be considered and melting and shedding would need to be taken into account to obtain more accurate t_{EPB} values.

$$E_{AI,R} = P_W Cp_{(TSR_{AI,R})} t_{EPB} + E_{DI,R} \quad (4)$$

$$E_{AI,M} = P_W Cp_{(TSR_{AI,M})} t_{EPB} + E_{DI,M} \quad (5)$$

$$t_{EPB} = (E_{DI,R} - E_{DI,M}) / \left[P_w\left(Cp_{(TSR_{AI,M})} - Cp_{(TSR_{AI,R})}\right)\right] \quad (6)$$

3. Results and discussion

3.1. Results

For each icing condition, *Cp* degradation, ice accumulation, final ice shapes for section D, ice induced power losses, rotor power characteristics, *Cp*(t), at the end of the event and energy payback times are presented in this section. In total 1176 ice shapes were generated for all icing events, with 180 ice shapes per timestep being analysed. Ice mass and *Cp* degradation were estimated considering all 1176 ice shapes, while the power characteristics and t_{EPB} were analysed investigating the ice shapes at the end of the icing events. All final ice shapes at the modelled blade locations are provided in the Supplementary Online Appendix, while in this section only the most heavily iced blade location has been presented (section D, see Fig. 1). Ice-induced power losses and total harvested energy before and after an event, considering all modelled blade sections, were the main parameters used for the comparison of alternative TSR_{DI} and TSR_{AI} strategies. Ice mass for each strategy on a single blade is shown, but aeroelastic effects and component loads are beyond the scope of this work as for similar icing conditions it has been shown that the effects on the structural loading from additional ice mass are minimal [14,16].

3.1.1. Event A

Event A has been simulated for wind speeds of 10, 7 and 5 m s^{-1} and ambient temperatures of −10 and −5 °C, resulting in 6 cases – A1010; A105; A710; A75; A510 and A55. E.g. A1010 represents the LWC, MVD and duration defined by Event A in Table 1, occurring with a wind speed of 10 m s^{-1} and an ambient temperature of −10 °C.

The deteoration of *Cp* for the whole simulated wind turbine rotor and the ice mass accumulation for each blade for all cases of Event A are presented on Fig. 4a–f. Alternative viable operational TSRs of 6.5–8 for wind speeds of 10 and 7 m s^{-1} (Fig. 4a–d) and TSRs of 9–10 for wind speed of 5 m s^{-1} (Fig. 4e and f) are shown. TSR values greater than TSR_R for a wind speed of 5 m s^{-1} are not considered for the analysis as it would result in a high V_{rel} and ice build-up (see Fig. 2a). As the ice accumulation rate is a function of the blade's relative velocity [9,14], less ice deposition is apparent when the ambient temperature increases and both the wind speed and the TSR decrease (see Fig. 4). The highest amount of accreted ice per blade is 11.5 kg for case A1010; the least is 4 kg for case A55. As the type of ice being formed can change from one type to another for the same icing case (rime to glaze) and it can vary along the blade of utility scale wind turbines, the power convergence efficiency does not degrade linearly. Depending on the type of accreted ice and the disturbance of the flow over the blade, the *Cp* decreases either gradually (A1010, A710 and A510) or more sharply (A105, A75 and A55).

Final ice shapes for blade Section D (see Fig. 1) are displayed on Fig. 5a–f. The ice shapes for A105, A75 and A55 are typical for glaze icing conditions. They are characterised by having a less conformal geometry to the aerofoil contour and the presence of one or two horns [26]. The shapes for A510 are typical for rime ice cases as they are more conformal to the aerofoil geometry. Higher energy losses are expected for glaze and mixed icing conditions [14]. As these shapes produce more complex wall bounded flow, the aerodynamic uncertainties from the simulations tend to be higher, which is represented by the greater *Cp* fluctuations obtained for events A105, A75 and A55 (Fig. 4b, d and f). Higher fidelity analyses over a smaller range of time steps are needed to further investigate these specific flow features and fluctuations in the results. For cases A1010, A710 (Fig. 5a and c) the ice shapes are representative for mix-type icing, being conformal to the aerofoil contour at first (rime) and subsequently forming horn-like protrusions. The flatter *Cp* profiles for Events A1010, A710 and A510 (Fig. 4a, c and e) are attributed to ice forming normal to the leading edge or on the pressure side of the aerofoil causing less aerodynamic disturbance [10] (see Fig. 5a,c and e).

Fig. 6a–f reveals how setting different TSR values can be used to minimise power losses during icing and maximise performance after an icing event ends. Specifically, the results show the power coefficients of the iced wind turbine at the end of the icing events for different TSR_{DI} values, and subsequent power coefficients that can be obtained with a new TSR_{AI} value. As expected, the minimum TSR_{DI} typically provides the best possible post-icing performance, due to less ice having deposited on the rotor blades. The exception is case A710, where the differences between alternative TSRs are negligible due to the relatively small accumulation of ice. For example, Fig. 6d shows that the turbine could be slowed down to a TSR_{DI} of 6.5 with TSR_{AI} increased to 8 to achieve a power coefficient of over 0.475. These results also highlight how significant the degradation of *Cp* can be for the TSR_R value of 7.5 (Fig. 6a–d) and that restoring TSR_{AI} to 7.5 would improve the power performance after icing in events A1010 and A105. To maximise the power output and minimise the icing losses for a wind speed of 5 m s^{-1}, both TSR_{DI} and TSR_{AI} should be 9 as it provides higher *Cp* at lower rotor rotational speeds, but the viability of this depends on the coupled electrical generator.

The time it would take to replace the lost energy for reducing the TSR during the icing event, t_{EPB}, is shown for Event A on Fig. 7a–f. It is noticeable how sensitive t_{EPB} is to variations in wind speed, ambient temperature and TSR operational regime. For Event A at wind speeds of 7 and 10 m s^{-1} (Fig. 7a–f), the most beneficial TSR_{DI} is 7 with TSR_{AI} set to either 7.5 or 8, which provides energy payback times of around 0.5–2.5 h. Interestingly, if the TSR_{AI} was to be restored to the turbines reference speed (TSR_R) of 7.5 after event A105, the only TSR_{DI} and resulting characteristics that could replace the lost energy would be $TSR6.5_{DI}$. For event cases A510 and A55, *Cp* is improved for a reduced TSR value both during and after the icing events, so there is no energy payback, and this suggests that the reference design strategy could be improved for non-icing conditions. As a result, the energy payback time appears negative in Fig. 7e and f.

3.1.2. Event B

In comparison to Event A, the *Cp* degradation for all Event B cases is more gradual due to a reduced ice accretion rate and more conformal ice shapes to the blade geometry (see Fig. 8a–h). The sudden *Cp* drop for B710 and B75 during the first hour of icing is an

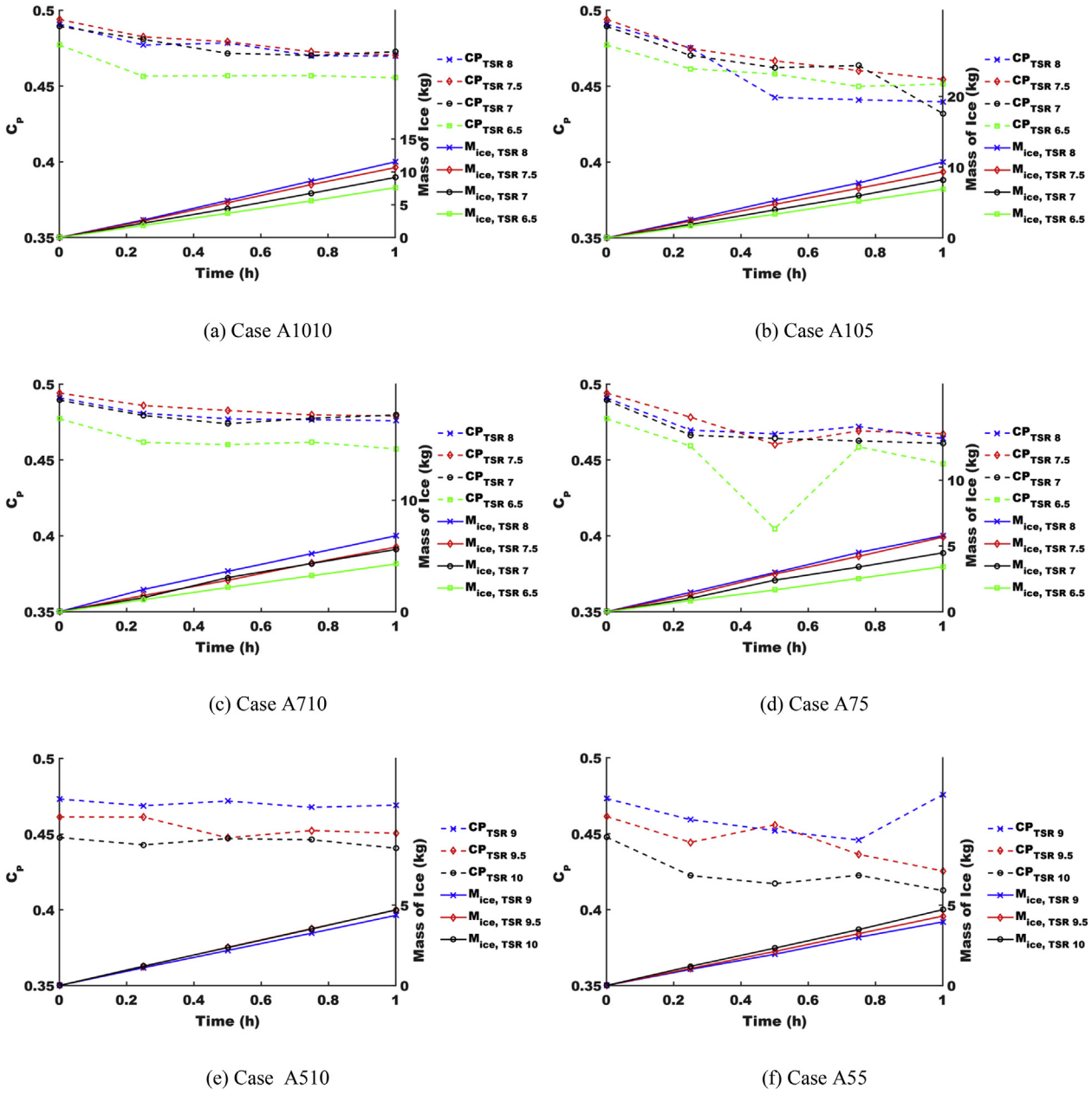

Fig. 4. a–f: Wind turbine power coefficient degradation and total ice mass accumulation per blade during events A1010 (a), A105 (b), A710 (c), A75 (d), A510 (e) and A55 (f).

interesting observation and can be attributed to the way the ice shapes form during the event. As the ice shapes are representative for rime and mixed-type icing, they are conformal to the clean geometry until the thermodynamic equilibrium changes on the air-ice boundary. It is apparent that before the thermodynamic equilibrium changes, the rime shapes during the first hour of icing are characterised by greater leading edge curvature slopes than the ice shapes at the end of the event. Due to the nature of the panel method algorithm, greater curvature slopes lead to reduced accuracy of the analysis. The aerodynamic uncertainties for B710 and B510 indicate ice shapes with increased curvature slopes near the leading edge region occurring during the 3rd hour of icing. This highlights the need for a greater fidelity aerodynamic analysis of such conditions.

The TSR_{AI} power characteristics for shapes produced during Event B cases are not particularly sensitive to changes in TSR_{DI}. Fig. 9a–d shows that only minimal performance improvements can be achieved after icing by slowing the rotor down during the icing event. Unlike for Event A, only event B75 results in a TSR_{DI} of 6.5 being the preferred option for post-icing operation. Similarly, the minimum TSR_{DI} for event B510 provides the most favourable power characteristics after icing. The maximum TSR_{DI} of 8 indicated as the best option for B1010 is likely due to the discrepancies of the aerodynamic analysis and the negligible differences in the aerodynamic performance of the produced ice shapes under these conditions and TSR_{DI} values.

The minimal performance improvement observed from reducing the TSR_{DI} indicates that the energy payback time will be long or unachievable. Reducing to a TSR_{DI} of 7 and increasing to a TSR_{AI} of 7.5 would have a long energy recovery time of 6h for B1010, 11.5h for B710 and 8.5h for B75. For $TSR6.5_{DI}$ this would increase to 19.5h, 21.3h and 16h for events B1010, B710 and B75, respectively.

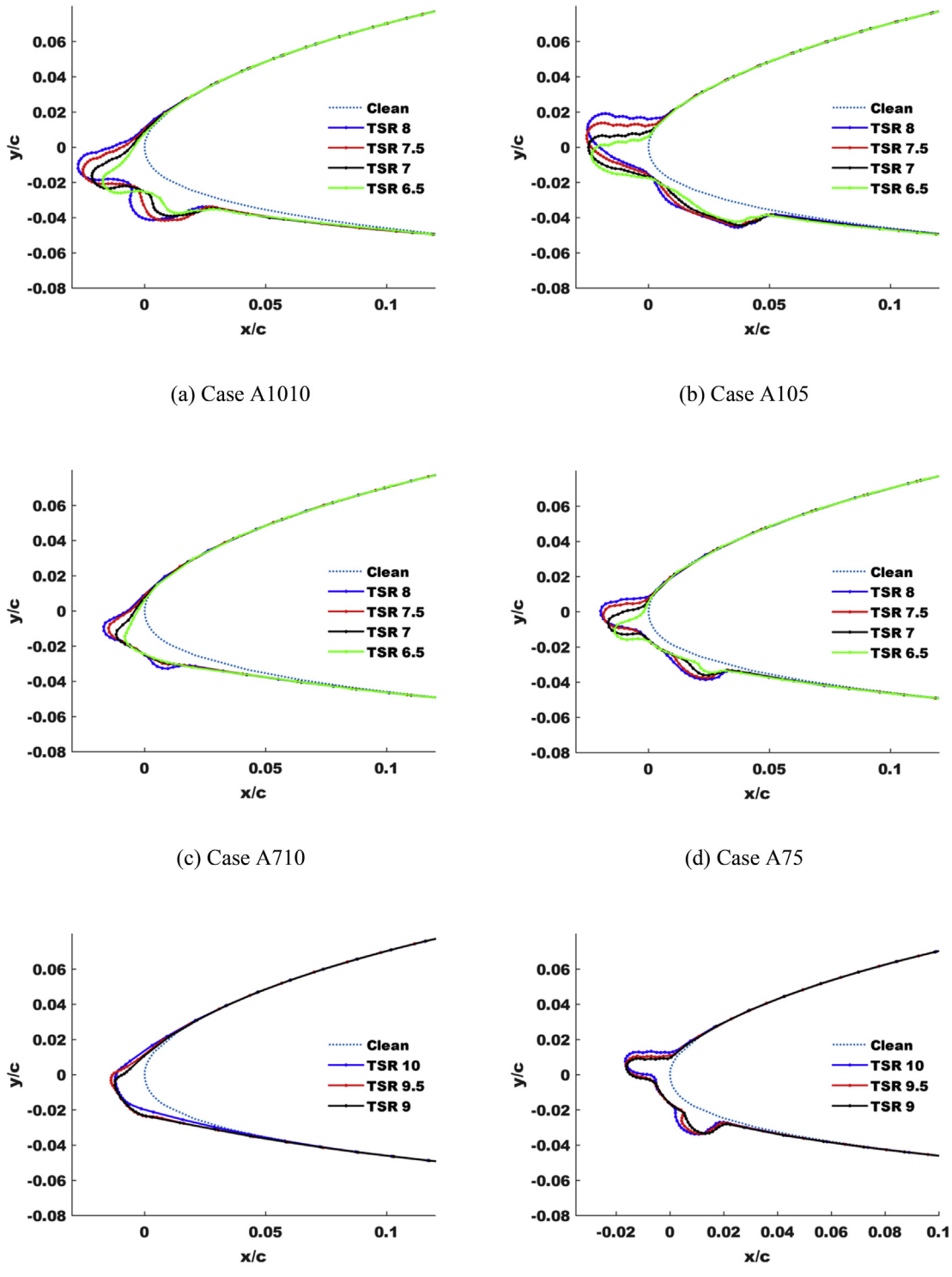

(a) Case A1010 (b) Case A105

(c) Case A710 (d) Case A75

(e) Case A510 (f) Case A55

Fig. 5. a–f: Ice shapes on Section D for event cases A1010 (a), A105 (b), A710 (c), A75(d), A510 (e) and A55 (f).

For some TSRs, t_{EPB} can reach extreme values (48–200h), which indicates that alternative ice mitigation approach should be considered or, if the power losses are too high, complete shutdown would be advisable. With a TSR_{DI} of 7.5 and 8 having very similar performance profiles for event B1010 and B710 (Fig. 9a and b) and $TSR8_{DI}$ slightly underperforming on average–but having a higher *Cp* at the end of the icing event (see Fig. 8a–c)–the short energy payback time indicated for $TSR8_{DI}$ on Fig. 10a and b should be neglected. During B510, the modified TSR strategies ($TSR9_{DI}$ and $TSR9.5_{DI}$) provide higher energy yield and less ice-build up than

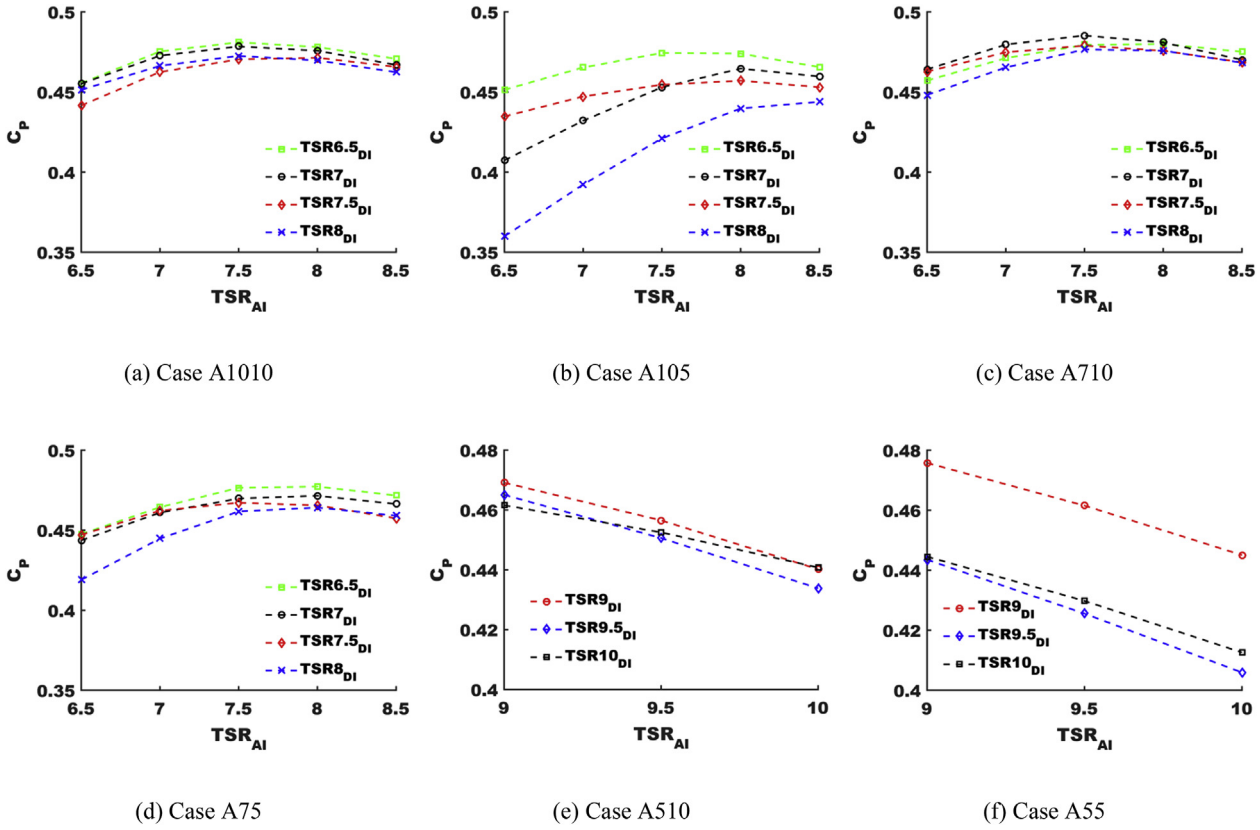

Fig. 6. a–f: Power characteristics of modified tip-speed ratio values after icing events A1010 (a), A105 (b), A710 (c), A75(d), A510 (e) and A55 (f).

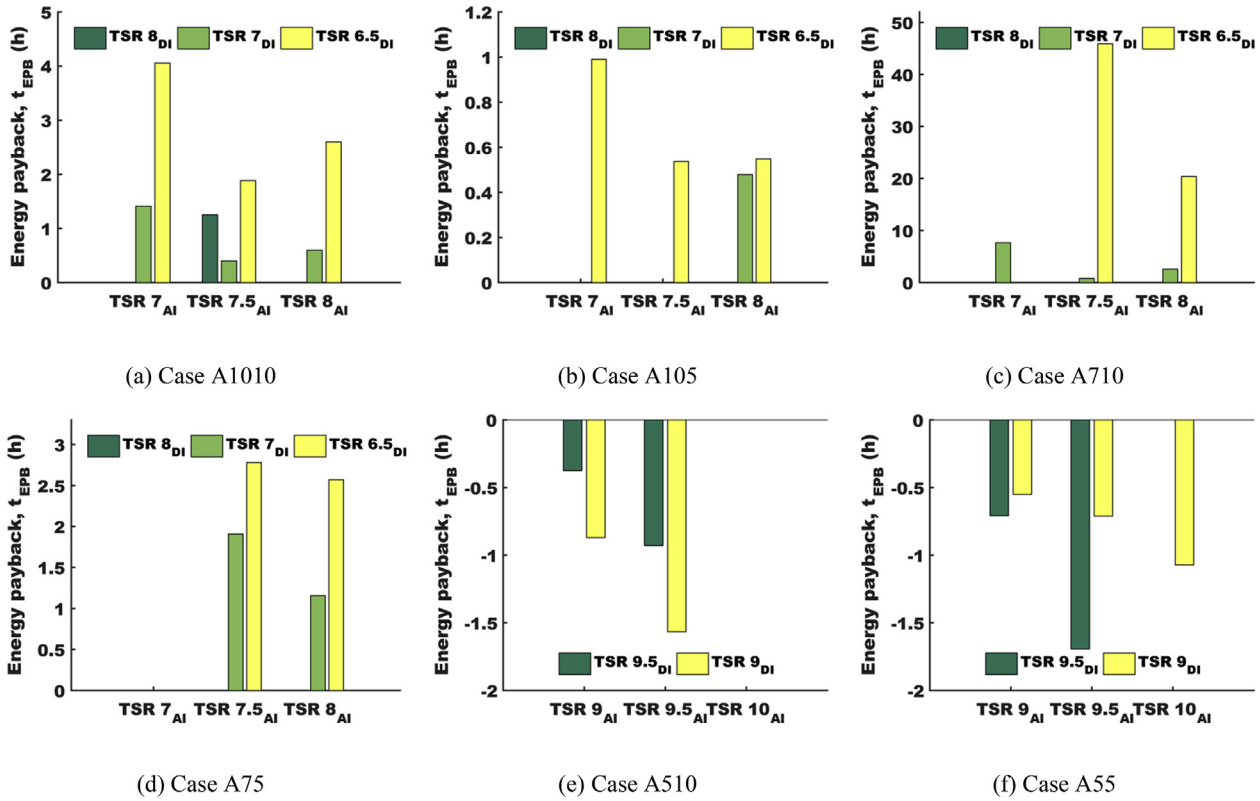

Fig. 7. a–f: Energy payback time for different tip-speed ratio after icing (TSR_{AI}) values for events A1010 (a), A105 (b), A710 (c), A75(d), A510 (e) and A55 (f).

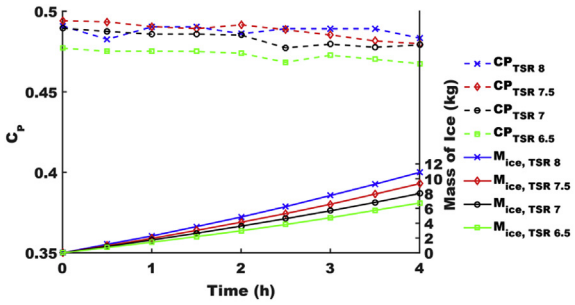

(a) case B1010

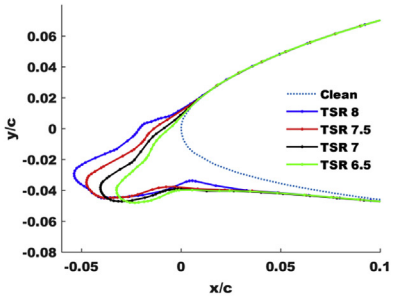

(b) case B1010

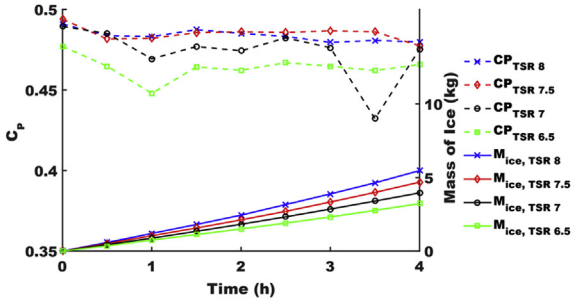

(c) Case B710

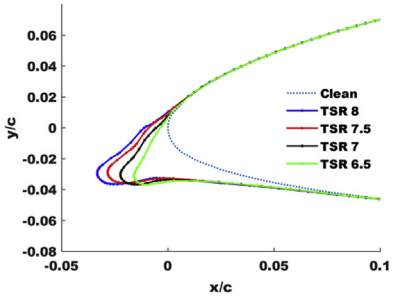

(d) Case B710

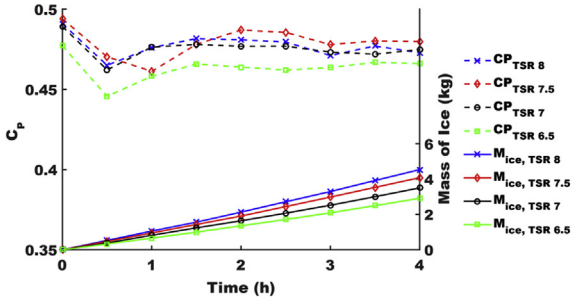

(e) Case B75

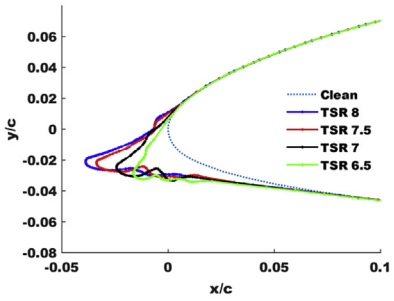

(f) Case B75

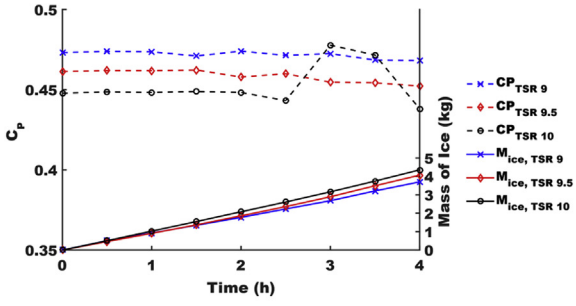

(g) Case B510

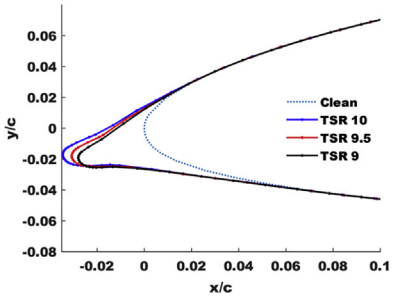

(h) Case B510

Fig. 8. a–h: Wind turbine Cp deteoration and ice accumulation per blade during events B1010 (a), B710 (c), B75 (e), B510 (g) and ice shapes on section D at the end of events B1010 (b), B710 (d), B75 (f), B510 (h).

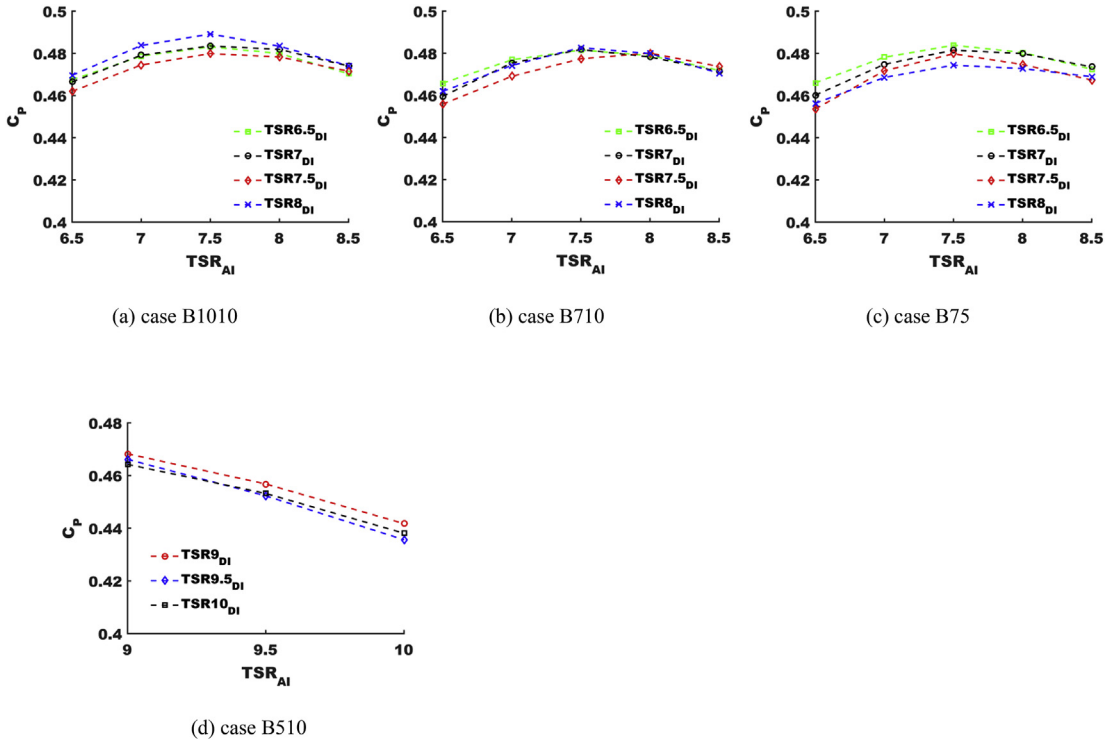

(a) case B1010 (b) case B710 (c) case B75

(d) case B510

Fig. 9. a–d: Power characteristics of modified tip-speed ratio values after icing events B1010 (a), B710 (b), B75 (c) and B510 (d).

operating at TSR_R resulting in a negative energy payback time.

3.1.3. Event C

Among Events A, B and C, Event C is characterised by having the lowest values for LWC and MVD and ice accretion rates. With Event C being simulated for a wind speed of 10 m s^{-1} and ambient temperatures of −5 and −10 °C, two cases are presented: C1010 and C105. Due to small ice build-up and shapes (approximately 0.15–0.4 kg for different TSR_{DI} values), the power losses are no greater than 1% over the duration of the 4-h icing events. In addition, the ice shapes are located on the pressure side of the leading edge of the blade (see Fig. 11), leading to increased drag but

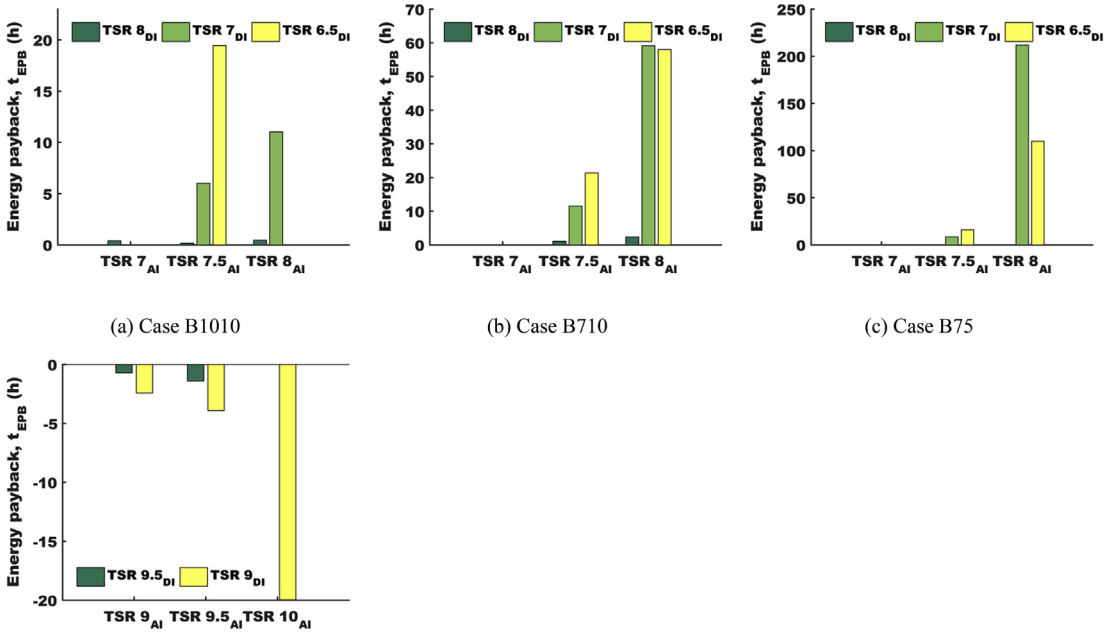

(a) Case B1010 (b) Case B710 (c) Case B75

(d) Case B510

Fig. 10. a–d: Energy payback time for different tip-speed ratio after icing (TSR_{AI}) values for events B1010 (a), B710 (b), B75(c) and B510 (d).

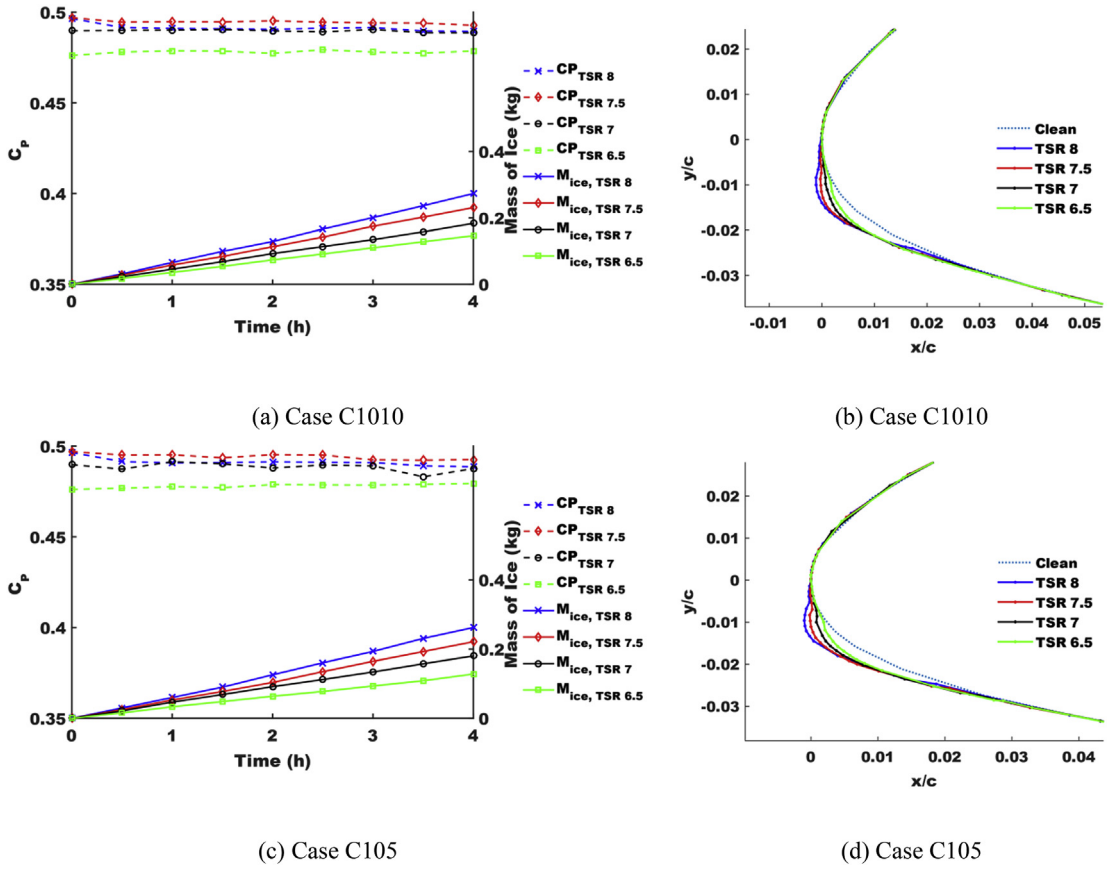

(a) Case C1010 (b) Case C1010

(c) Case C105 (d) Case C105

Fig. 11. a–d: Wind turbine Cp deteoration and ice accumulation per blade during events C1010 (a) and C105 (c) and ice shapes on section D at the end of events C1010 (b) and C710 (d).

minimal changes in lift [10].

From the energy payback time analysis, it can be concluded that the best option for operation for event C is to maintain operation at the reference TSR_R (i.e. 7.5). Energy payback time for all alternative operational strategies is relatively high for Event C, as there are minimal changes in *Cp* for different TSR_{DI} values (Fig. 12a and b) and the ice deposition is low. For instance, by setting the TSR_{DI} to 7 and then operating at a TSR of 7.5 the energy recovery time would be either 24h (A105) or 14h (A1010) (see Fig. 13a and b).

3.2. Further work

As there are many different icing events that can last for a few hours to several days, the viability of the different operational strategies proposed in this study still needs further investigation. The current analysis utilised XFoil, which enabled the aerodynamic performance of a large number of different ice shapes to be analysed with relatively low computation effort. However, the suggested ideal tip-speed ratio strategy for each event highly depends on the accuracy of the predicted aerodynamic penalties caused by ice build-up. In this study, the aerodynamic performance predictions are more reliable and accurate for the generated ice shapes without extreme irregularities and high curvature at the leading edge. Therefore, for the analysis of icing events leading to more irregular shapes, higher fidelity tools, such as Navier-Stokes equation-based solvers, are required.

A predictive model based on XFoil, or another tool that combines a panel method and integral boundary layer equations, could be developed to inform wind turbine controllers in real time, which would have significant benefits for wind farm operations. However, detection of ice accretion on wind turbines remains a challenge. This study has also highlighted some of the uncertainties and limitations of the panel method, so further work will be carried out to experimentally characterise and investigate them in more detail, so that improved predictive algorithms can be developed in the future.

The approach taken in this study of determining an energy payback time for different TSR operational strategies was found to be useful for both comparing the effectiveness of different strategies and indicating when normal operation can be maintained, or a different ice mitigation technique would be needed (e.g. an anti/de-icing system). Additional research will be carried out to evaluate the energy requirements to size and evaluate potential net energy gains/losses of using an anti-icing system in comparison to the alternative TSR strategies investigated for the events proposed in this study. Moreover, it will be interesting to consider how the model for predicting energy payback time can be modified to consider ice reduction mechanisms – such as melting, shedding and sublimation. If modelled, the ice mass would reduce after an icing event and the *Cp* would tend towards its clean blade value. However, this would be dependent on the weather conditions and the structural vibrations. In addition, the estimated energy payback times could be shorter if the ice deposition for an alternative operational strategy reduced faster than the ice accumulated for $TSR_{DI,R}$, but further investigations are required to accurately model this. The model could also be extended do determine which strategy is the most effective when vibration and structural analysis is incorporated. The viability of a TSR strategy would depend on the

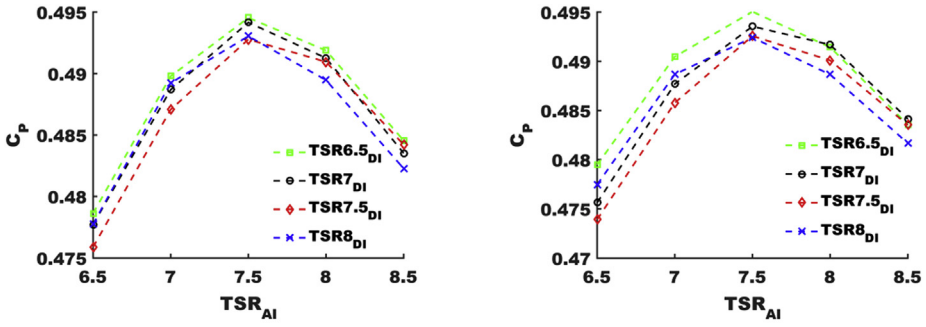

(a) Case C1010 (b) Case C105

Fig. 12. a–b: Power characteristics of modified tip-speed ratio values after icing events C1010 (a) and C105 (b).

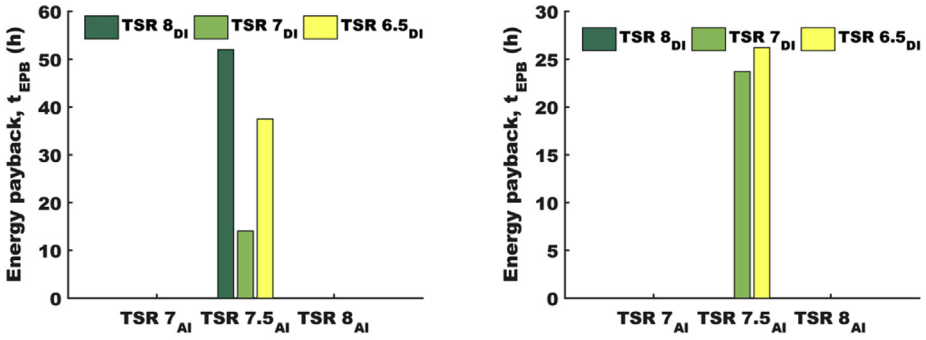

(a) Case C1010 (b) Case C105

Fig. 13. a–b: Energy payback time for different tip-speed ratio after icing (TSR_{AI}) values for events C1010 (a) and C105 (b).

wind turbine type, local weather parameters and structural damage limitations. As rotational speed would actually decrease on variable-speed and variable-pitch wind turbines due to ice formation, a further improvement to the model could be achieved by modelling the transient behaviour of the TSR during ice build-up. This will be particularly beneficial when analysing long severe icing events.

4. Conclusion

This paper examined the effectiveness of rotational speed modifications for the NREL 5 MW reference wind turbine during icing conditions. The turbine was simulated for three icing events, three wind speeds and two ambient temperatures, resulting in 12 different cases. To compare the effectiveness of each strategy, an energy payback time parameter was modelled to determine when slowing a wind turbine down during an icing event would provide overall more energy than a conventional strategy. The obtained results suggested that alternative strategies for mitigating ice losses, realised by tip-speed ratio modifications, are most effective for short and severe icing events. For LWC of 5×10^{-4} kg m^{-3} and MVD of 25×10^{-6} m, the energy that is lost due to reducing the tip-speed ratio can be recovered within 0.5–2.5 h post-icing event, thereby reducing the power losses by 7–23% and ice mass accreted on each blade by 20–30%. However, for longer and milder events, the energy recovery time is significantly longer (around 10–28h) suggesting the reference design strategy should be maintained. Additionally, the possibility for applying the TSR modification strategies should be considered carefully, as only limited ice mass would be acceptable due to structural constraints. Furthermore, the need for higher fidelity analysis tools is apparent for longer icing events, with XFoil being more effective for modelling short rime and glaze icing conditions, which do not result in severe horn-like shapes. Where previous wind turbine icing studies have tended to focus on just ice-induced power losses, this study has demonstrated the importance of considering a wind turbine blade's power characteristics and energy production throughout an icing event and performance once an icing event ends. The energy payback time method presented can identify which tip-speed ratio modifications can be used during and after an icing event, provided local meteorological conditions can be accurately predicted. Thus, this work will be of significant interest to wind turbine operators working in cold climate locations.

Appendix A. Supplementary data

Supplementary data to this article can be found online at https://doi.org/10.1016/j.renene.2019.08.023.

References

[1] Anon, Global Wind Report, GWEC, 2018, pp. 16–60.
[2] V. Lehtomaki, Emerging from the Cold, Wind Power, 2019, p. 1, 2016, https://www.windpowermonthly.com/article/1403504/emerging-cold.
[3] G. Fortin, J. Perron, A. Ilinca, Behaviour and modeling of cup anemometers under icing conditions, IWAIS 11 (2005) (Montreal).
[4] V. Turkia, S. Huttunen, T. Wallenius, Method for Estimating Wind Turbine Production Losses Due to Icing, 2013.
[5] A. Krenn, P.J. Jordaens, M. Wadham-Gagnon, N. Davis, N. Clausen, V. Lehtomaki, et al., Wind Energy in Cold Climates Available Technologies -

Report, 2016.
[6] R.E. Bredesen, R. Cattin, N. Clausen, N. Davis, P.J. Jordaens, Z. Khadri-Yazami, et al., Wind Energy Projects in Cold Climates, 2017.
[7] A Ilinca O Parent, Anti-icing and de-icing techniques for wind turbines: critical review, Cold Reg. Sci. Technol. 65 (2011) 88–96.
[8] N. Dalili, A. Edrisy, R. Carriveau, A review of surface engineering issues critical to wind turbine performance, Renew. Sustain. Energy Rev. 13 (2007) 428–438.
[9] L. Battisti, Chapter 4 Icing Process, Wind Turbines in Cold Climates, Springer, Switzerland, 2015, pp. 177–248.
[10] M. Bragg B, A. Broeren P, L. Blumenthal A, Iced-airfoil aerodynamics, Prog. Aerosp. Sci. (2005) 323–362.
[11] B. Tammelin, M. Cavaliere, H. Holttinen, C. Morgan, H. Seifret, K. Santti, Wind Energy Production in Cold Climates, WECO, 2000.
[12] T. Laakso, I. Baring-Gould, M. Durstewitz, R. Horbaty, A. Lacroix, E. Peltola, et al., State-of-the-art of Wind Energy in Cold Climates, 2010.
[13] B. Tammelin, H. Seifret, Large Turbines Go into Cold Climate Regions, EWEC 2001, Copenhagen, 2001.
[14] M. Etemaddar, M. Hansen, T. Mo, Wind turbine aerodynamic response under atmospheric icing conditions, Wind Energy 17 (2012) 241–265.
[15] N. Davis, Hahmann AN, N. Clausen, M. Zagar, Icing Impacts on Wind Energy Production, DTU, 2014.
[16] L. Hu, X. Zhu, C. Hu, J. Chen, Z. Du, Wind turbine ice distribution and load response under icing condition, Renew. Energy 113 (2017) 608–619.
[17] R. Cattin, Icing of Wind Turbines, Elforsk 12 (2012) 13, 23.
[18] M. Homola, M. Virk, P.J. M Nicklasson, Performance losses due to ice accretion for a 5 MW wind turbine, Wind Energy 15 (2012) 379–389.
[19] A. Zanon, M. Gennaro De, H. Kuhnelt, Wind energy harnessing of the NREL 5 MW reference wind turbine in icing conditions under different operational strategies, Renew. Energy 115 (2018) 760–772.
[20] D. Brillembourg, Turbines under atmospheric icing conditions - ice accretion modelling, aerodynamics, and control strategies for mitigating performance degradation, Wind Energy 20 (2013) 601–617.
[21] W. Wright, User's Manual for LEWICE Version 3.2, 2008.
[22] W. Wright B, Validation Results for LEWICE 3.0, 2005.
[23] D. Marten, J. Wendler, Qblade Guidelines, 2013.
[24] M. Drela, XFOIL: an Analysis and Design System for Low Reynolds Number Airfoils, Low Reynolds Number Aerodynamics, 1989.
[25] J. Jonkman, S. Butterfield, W. Musial, G. Scott, Definition of a 5-MW Reference Wind Turbine of Offshore System Development, 2009.
[26] G. Poots, Ice and Snow Accretion on Structures, first ed., Research Studies Press, Exeter, 1996.
[27] M.C. Pederson, H. Sorenson, N. Swytink-Binnema, B. Martinez, T. Condra, Measurements from a cold climate site in Canada: boundary conditions and verification methods for CFD icing models for wind turbines, Cold Reg. Sci. Technol. 147 (2018) 11–21.
[28] S. Cober G, G. Isaac A, J. Strapp W, Aircraft icing measurement in east coast winter storms, J. Appl. Meteorol. 34 (1994) 88.
[29] F. Lamraoui, G. Fortin, R. Benoit, J. Perron, C. Masson, Atmospheric icing impact on wind turbine production, Cold Reg. Sci. Technol. 100 (2014) 36–49.
[30] W. Lewis, A flight investigation of the meteorological conditions conducive to the formation of ice on airplanes, Natl. Advis. Comm. Aeronaut. 1393 (1947) 25.
[31] L. Chen, B. Tan, G. Kvamsto Nils, M Johannessen Ola, Winter cyclone/anti-cyclone activity over China and its relation to upper tropospheric jets, Tellus A Dyn. Meteorol. Oceanogr. 66 (2014).